DOI: 10.1002/zaac.201300229

Dehydration of the Sorel Cement Phase $3Mg(OH)_2{\cdot}MgCl_2{\cdot}8H_2O$ studied by in situ Synchrotron X-ray Powder Diffraction and Thermal Analyses

Tomče Runčevski,[a] Robert E. Dinnebier,*[a] and Daniela Freyer*[b]

Keywords: Magnesia cement; $Mg(OH)_2$-$MgCl_2$-H_2O system; Crystal structure; Dehydration; Decomposition

Abstract. Dehydration is an important process which affects the chemical, physical and mechanical properties of materials. This article describes the thermal dehydration and decomposition of the Sorel cement phase $3Mg(OH)_2{\cdot}MgCl_2{\cdot}8H_2O$, studied by in situ synchrotron X-ray powder diffraction and thermal analyses. Attention is paid on the determination of the chemical composition and crystal structure of the lower hydrates, identified as the phases $3Mg(OH)_2{\cdot}MgCl_2{\cdot}5.4H_2O$ and $3Mg(OH)_2{\cdot}MgCl_2{\cdot}4.6H_2O$. The crystal structure of $3Mg(OH)_2{\cdot}MgCl_2{\cdot}4.6H_2O$ is solved and refined by the Rietveld method and a structural model for the $3Mg(OH)_2{\cdot}MgCl_2{\cdot}5.4H_2O$ phase is given. These phases show statistical distribution of water molecules, hydroxide and chloride anions positioned as ligands on the magnesium octahedra. A structural scheme of the temperature induced transformations in the thermal range from 25 to 500 °C is presented.

Introduction

The reaction of caustic magnesium oxide with concentrated solution of magnesium chloride gives binder phases known as Sorel cements, with general formula $x Mg(OH)_2{\cdot}y MgCl_2{\cdot}z H_2O$ (abbreviated as *x*-*y*-*z*).[1–6] The two most important Sorel phases are the 3-1-8 phase, which crystal structure was reported in 1953 by *de Wolff* and *Walter-Levy*,[7] and the 5-1-8 phase, which crystal structure was solved by *Sugimoto* et al.[8]

The Sorel cements are important materials showing many superior properties including high compressive and flexural strength, high fire resistance, low thermal conductivity, high resistance to abrasion, etc. As a result, they are used as floor material, bonding agent in wet stones applications, for production of artificial ivory, grindstones, cast stones, tiles and other materials. The 3-1-8 cement phase is used as barrier construction materials in salts formations because it is stable toward Mg^{2+} containing salts and their solutions. Due to this quality, the material is tested for application in final disposal concepts for radioactive wastes.[9]

The knowledge of the high-temperature behavior, especially the dehydration of cementitious materials, is crucial for optimizing their performance. Among the first studies on 3-1-8 phase are those reported by *Cole* and *Demediuk,* according to which the composition of the phase changes on heating from 3-1-8 to 3-1-5 (at 145 °C), 3-1-4 (at 170 °C) and 3-1-0 (at 220 °C).[10] The thermal investigations performed by *Xia* et al. also showed a multistep dehydration process.[11] In situ crystallographic studies on Sorel phases were performed by *Christensen* et al.[12,13] *Dinnebier* et al. reported the crystal structures of the 9-1-4,[14] 2-1-2 and 2-1-4[15] high temperature phases, as well as the crystal structure of the anhydrous phases formed by heating of the 3-1-8 and 5-1-8 phases.[16] Further heating (above 400 °C) of Sorel cements results in formation of magnesium oxide.

In order to fill the gap of structural knowledge of the dehydration and decomposition behavior of the 3-1-8 phase, detailed crystallographic and thermal studies were undertaken under the scope of our on-going investigations on basic magnesium salt hydrates.[14–20] The dehydration processes were followed by in situ synchrotron X-ray powder diffraction (XRPD), thermogravimetric (TG) and differential thermal (DTA) analyses. A structural scheme of the thermal behavior of the 3-1-8 magnesia binder phase, in a wide temperature range from 25 to 500 °C, is presented.

Results and Discussion

High Temperature Dehydration: in situ XRPD

The process of the 3-1-8 dehydration was followed in situ by synchrotron XRPD. Figure 1 presents the 2D projection (simulated heating Guinier plot) of the observed scattered intensity as a function of diffraction angle and temperature. This temperature interval (from 50 to 170 °C) was chosen because previous studies indicated formation of two lower hydrates in this range and the processes at higher temperatures were already reported in a previous study.[16] Three regions can be observed in the 2D projection: the first one ($T < 100$ °C) corresponding to the 3-1-8 phase, and the following two

* Prof. Dr. R. E. Dinnebier
Fax: +49-711-689-1502
E-Mail: r.dinnebier@fkf.mpg.de
* Dr. D. Freyer
Fax: +49-3731-39-4058
E-Mail: Daniela.Freyer@chemie.tu-freiberg.de
[a] Max Planck Institute for Solid State Research
Heisenbergstrasse 1
70569 Stuttgart, Germany
[b] TU Bergakademie Freiberg
Institute of Inorganic Chemistry
Leipziger Strasse 29
09596 Freiberg, Germany

Zeitschrift für anorganische und allgemeine Chemie ZAAC Journal of Inorganic and General Chemistry

(100 °C < T < 130 °C and 130 °C < T < 170 °C) to newly formed lower hydrates. The overlap of the diffraction peaks from different phases at the borders of the thermal regions indicates that the phase transitions among them are not sharp, but occur gradually in a given thermal interval with continuous water loss.

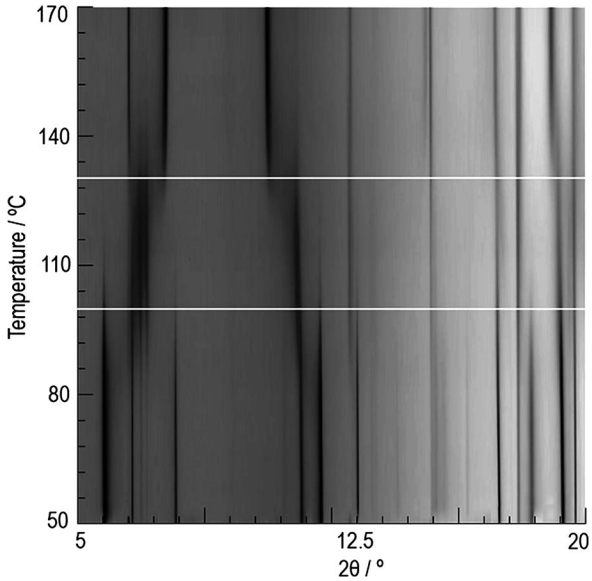

Figure 1. Two-dimensional projection (simulated heating Guinier plot) of the observed scattered X-ray intensity for the 3-1-8 phase as a function of diffraction angle and temperature. Three temperature ranges are identified and separated by the white lines: the first one corresponding to the 3-1-8 phase, and the following two to the lower hydrate phases formed on heating.

High Temperature Dehydration: Thermal Analyses

In order to determine the temperature ranges of formation of the lower hydrates, as well as to calculate the amount of water lost during the dehydrations, combined TG/DTA analyses were performed. The water loss was shown to be kinetically controlled and highly depended on the heating rate and environmental conditions as compared to previously reported results.[10,11] Figure 2 presents the thermal analysis measurement performed with the same heating rate as the one used during the in situ X-ray diffraction data collection (3 K·min^{-1}), enabling comparison of the experimental results obtained by the structural and thermoanalytical studies (it should be noted, however, that the sample environment during the experiments was comparable, for the thermal analysis measurements an open crucible easily covered with a platinum metal disc was used as well as the diffraction data were collected from a sample filled in an open glass capillary).

The dehydration of the 3-1-8 phase starts at about 80 °C. Between 115 and 120 °C the slopes of DTA and DTG curves are nearly zero, which indicates the formation of the first stationary lower hydrate. The TG curve shows that 2.6 ± 0.04 water molecules (Δm = –11.4 ± 0.1 %) are lost up to this point and the newly formed phase has 3-1-5.4 stoichiometry. In the 2D in situ XRPD plot the formation of this phase starts at

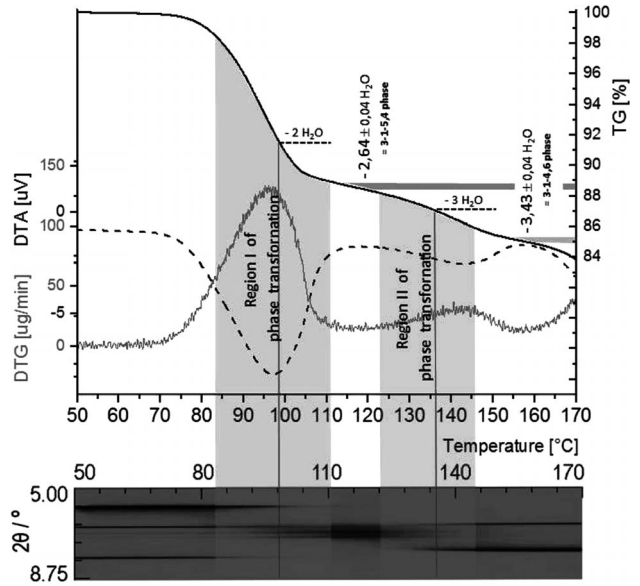

Figure 2. Overlay of thermal analyses and 2D XRPD plot: *Upper panel:* DTA and DTG curves (left axis) and TG curve (right axis). *Lower panel:* Section of the two-dimensional projection of the observed scattered X-ray intensity as a function of diffraction angle and temperature. The two temperature regions of phase transformations and steady phase states are highlighted.

about 90 °C, it is completed at about 110 °C and exists up to 140 °C.

By further heating, additional, continuous water loss is evidenced accompanied by smaller endothermic effect (as compared to the one of the first phase transformation). The slopes of DTA and DTG curves are nearly zero in the temperature region between 155 and 160 °C, where the second lower hydrate is the dominant phase. At this point, the weight loss reaches a value of –14 ± 0.1 %, which corresponds to the loss of 3.4 ± 0.04 water molecules in respect to the starting 3-1-8 phase, thus the second formed phase has a 3-1-4.6 stoichiometry.

Heating at higher temperatures than 200 °C leads to the formation of two coexisting anhydrous magnesium hydroxychloride solid solutions with general chemical formula $Mg(OH)_xCl_y$ where $x + y = 2$. For the given compositions $Mg(OH)_{1.7}Cl_{0.3}$ and Mg(OH)Cl the crystal structures were reported.[16] These phases decompose into magnesium oxide at temperature higher than 400 °C (Figure 3). Magnesium oxide is the final dehydration/decomposition product of the Sorel phases, having a melting temperature above 2800 °C.

In order to clarify whether the mass loss is solely due to water loss or also due to hydrolysis reaction (that is removal of HCl) a second thermal analysis ran was performed, wherein the obtained gas phase was tested in respect of containing amounts of HCl. The presence of HCl was evidenced as decomposition product only at temperatures above 350 °C.

The thermal transformations of the 3-1-8 phase up to magnesium oxide, via intermediate formation of two lower hydrates and two hydroxychloride solid solutions, are summarized in Equations (1–4) and the thermal effects are displayed on the TG/DTA curve presented in Figure 3.

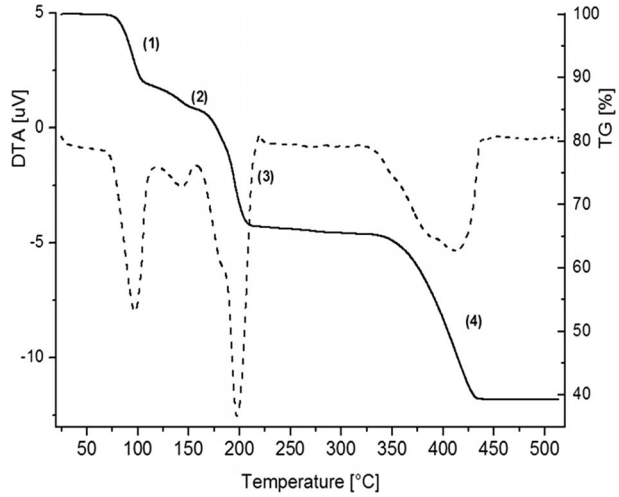

Figure 3. TG/DTA analysis curves of the 3-1-8 phase. The steps in the TGA curve correspond to Equations (1) to (4).

$$3\ Mg(OH)_2{\cdot}MgCl_2{\cdot}8H_2O \rightarrow 3Mg(OH)_2{\cdot}MgCl_2{\cdot}5.4H_2O + 2.6H_2O \quad (1)$$

$$3Mg(OH)_2{\cdot}MgCl_2{\cdot}5.4H_2O \rightarrow 3Mg(OH)_2{\cdot}MgCl_2{\cdot}4.6H_2O + 0.8H_2O \quad (2)$$

$$3Mg(OH)_2{\cdot}MgCl_2{\cdot}4.6H_2O \rightarrow 4[Mg(OH)_{x>1.67}Cl_{y<0.33} + Mg(OH)_{x<1.5}Cl_{y>0.5}] + 4.6H_2O \quad (3)$$

$$4[Mg(OH)_{x>1.67}Cl_{y<0.33} + Mg(OH)_{x<1.5}Cl_{y>0.5}] \rightarrow 4MgO + 2\ HCl + 2H_2O \quad (4)$$

Structural Changes on Dehydration

Although the crystal structure of the 3-1-8 phase has been known for almost 60 years, to the best of our knowledge, there are no crystal structure descriptions of the phases formed at the early stages of thermal decomposition, or the lower hydrates. The main reason for this gap of information in the crystal chemistry of the Sorel phases is the fact that these materials do not exist in form of crystals suitable for single crystal diffraction and powder diffraction is the most suitable method for crystal structure solution and refinement. Beside the intrinsic difficulties in using powder diffraction for structure solution, these phases exhibit severe defects and pronounced stacking faults, making the process an even bigger challenge.

As explained by *de Wolff* and *Walter-Levy*,[7] the crystal structure of the 3-1-8 phase at ambient conditions is built of MgO_6 octahedra forming infinite double chains, running in the direction of the crystallographic *b*-axis. The interchain region accommodates chloride anions and water molecules, found at two different positions in the unit cell. The crystal packing of this phase is presented in Figure 4a.

During heating, dehydration of the 3-1-8 phase takes place and part of the water molecules leaves the structure, as shown by thermoanalytical studies. After the first dehydration step, a first lower hydrate is formed in the temperature range from 115 to 120 °C.

This phase is characterized by very low crystallinity and pronounced stacking defects, which are visually observable in the shape and intensities of the diffraction pattern, which is

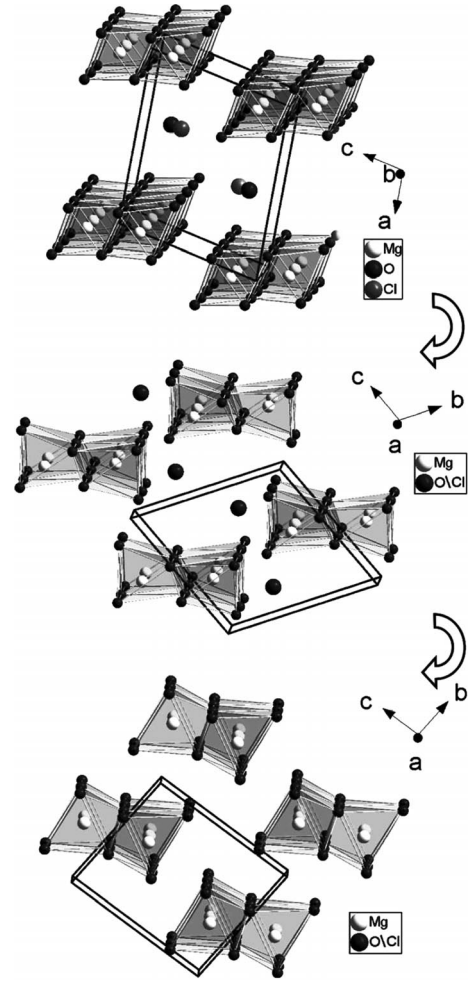

Figure 4. Crystal packing diagrams of the a) 3-1-8 (top), b) 3-1-5.4 (middle) and c) 3-1-4.6 phases (bottom). Semi-transparent magnesium octahedra characterized by statistical distribution of the anions are drawn. It should be noted that only a tentative model of the crystal structure for the 3-1-5.4 phase is presented (see Exp. Sect.).

given in Figure 5. As a result, after many trials, only a tentative model of the crystal structure was derived (see the experimental part for details), which could not be subjected to unconstrained and unrestrained Rietveld refinement. The structural model is shown in Figure 4b and presents an expected and logical intermediate phase of 3-1-8 and the second lower hydrate. According to the thermal analyses, the stoichiometry of this phase is 3-1-5.4. The structure solution indicates that there is statistical distribution of chloride and oxygen species, positioned at the same crystallographic position in the unit cell.

Further heating of the 3-1-5.4 phase results in additional loss of water molecules and according to the thermal analysis the stoichiometry changes to 3-1-4.6 (Figure 4c). The diffraction data quality of this phase was higher than the former hydrate, still the peaks shape and intensities indicated the presence of staking faults and similar defects. Fortunately, the crystal structure could be solved and subsequently refined by the Rietveld method. In this phase all water molecules, hydroxide and chloride anions are statistically distributed at the edge positions of the magnesium octahedra, and there are no atoms in in-

Zeitschrift für anorganische und allgemeine Chemie ZAAC Journal of Inorganic and General Chemistry

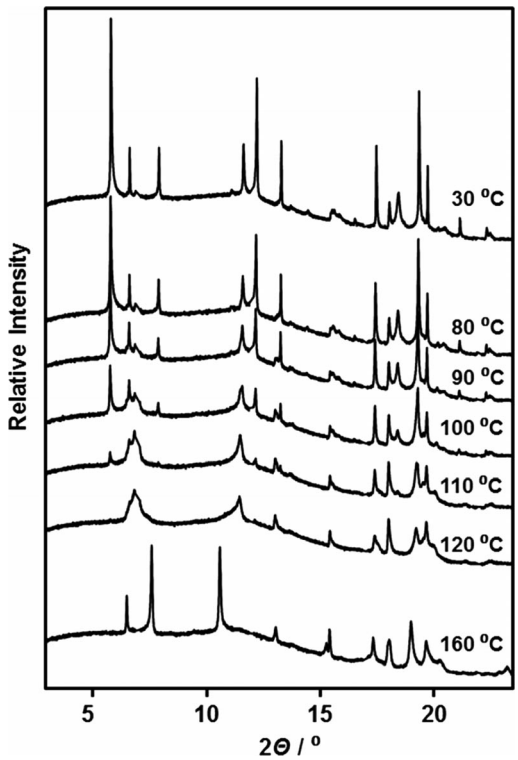

Figure 5. Selection of diffraction patterns obtained upon heating of the 3-1-8 phase (pattern at 30 °C). With increasing temperature a phase transformation takes place accompanied by significant lowering of data quality (see the diffraction pattern at 120 °C, corresponding to the first-formed lower hydrate). Subsequent heating results in another phase transition and better data quality (see the diffraction patter at 160 °C, corresponding to the second-formed lower hydrate).

terchain positions. Due to the low data quality and the statistical distribution, during the Rietveld refinement the occupancy values of the water molecules, hydroxide and chloride anions were constrained to chemically expected values, giving the 3-1-4.6 stoichiometry, as obtained by the TG/DTA measurement.

The figures of merit of the constrained refinement were slightly higher (≈ 0.5 %) as compared to the unconstrained refinement, which resulted in significantly different stoichiometry (3.3-0.7-4). Taken the low diffraction data quality, the constrained, chemically reasonable model is preferred.

In order to calculate the changes of phase amounts in the course of the dehydration processes, quantitative parametric Rietveld analysis was performed (see the Experimental Section for details). Figure 6 shows the phase evolution in the given temperature range (from 50 to 170 °C with a heating rate of 3 $K \cdot min^{-1}$). From room temperature to 100 °C the 3-1-8 phase is the only phase present; from 100 to 118 °C there is mixture of the 3-1-8 and 3-1-5.4 phases. The 3-1-5.4 phase occurs in a short temperature interval (118–123 °C) and after that exist in a mixture with the 3-1-4.6 phase (up to 160 °C). At temperatures greater than 170 °C only the 3-1-4.6 phase is present.

Conclusions

Using in situ synchrotron powder X-ray diffraction and thermal analyses (TG/DTA) the high temperature behavior of the

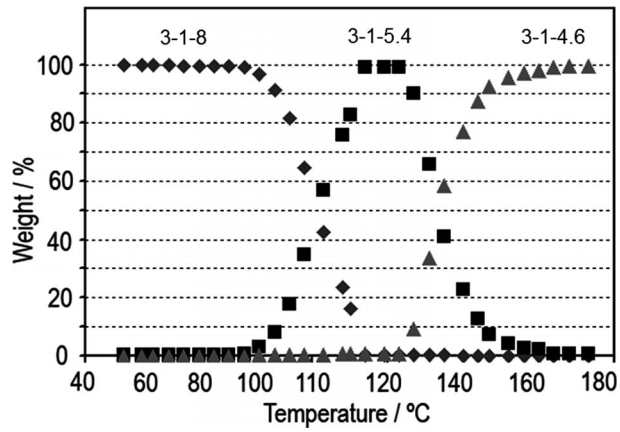

Figure 6. Quantitative parametric Rietveld analysis performed on data collected in situ on the course of the dehydration process of the 3-1-8 phase and the formation of the two lower hydrates.

Sorel cement phase 3-1-8 in the temperature region from 25 to 500 °C is studied and structurally and thermally characterized. By heating of the 3-1-8 phase, the first lower hydrate 3-1-5.4 is formed. Further heating results in additional loss of the interchain water molecules and the second lower hydrate with stoichiometry 3-1-4.6 is obtained. Above 200 °C the lower hydrates decompose in (minimum two) anhydrous magnesium hydrochloride solid solutions [$Mg(OH)_xCl_y$ with $x + y = 2$]. At temperatures above 400 °C further decomposition takes place and magnesium oxide is obtained as final product.

Accordingly, the following dehydration/decomposition Scheme of the 3-1-8 Sorel cement phase can be established: 3-1-8 (up to ca. 80 °C) → 3-1-5.4 (up to ca. 120 °C) → 3-1-4.6 (up to ca. 160 °C) → $Mg(OH)_{x>1.67}Cl_{y<0.33}$ + $Mg(OH)_{x<1.5}Cl_{y>0.5}$ (up to ca. 400 °C) → MgO (up to ca. 2800 °C).

Experimental Section

Phase Preparation

The initial 3-1-8 phase was prepared by a setting reaction of MgO (company Magnesia, MgO-Typ 2923, pure) with magnesium chloride solution ($MgCl_2 \cdot 6H_2O$, Fluka p.a., dissolved in deionized water (before use the water was boiled to remove the CO_2) in appropriate stoichiometrical formulation. After hardening process the sample was powdered and recrystallized from a 4 molal magnesium chloride solution for two months. Afterwards, the filtered solid was purified by washing two times with deionized cold water ($T < 5$ °C). To remove the adherent water the sample was washed with cold ethanol.

X-ray Data Collection

The powder diffraction data were collected in the temperature range from 50 to 170 °C using the high-resolution powder diffractometer at the I11 beamline, located at the British national synchrotron facility, Diamond Light Source. The wavelength of radiation was determined from a silicon standard to be 0.826401(3) Å. The beamline setup and characteristics are described in the literature.[21,22] The sample was placed in an open glass capillary (Hilgenberg glass No. 50), which was

spun during data collection for better particle statistics. The scans at each temperature were written continuously with 3 K·min^{-1} and 14 s per frame. The two-dimensional projection of the scattered X-ray intensity as a function of temperature and diffraction angle (Figure 1) was made using the software Powder3D.[23]

Crystal Structure Solution and Refinement

On heating two lower hydrates with previously unknown crystal structures were identified. The powder patterns were indexed (using the program suite TOPAS Version 4.2)[24] and the extinctions found pointed at $P1$ or $P\bar{1}$ as possible space groups. The peak profiles and precise lattice parameters were determined by a Pawley fit[25] using the fundamental parameter approach. Chebyshev polynomials were used for the modeling of the background.

Figure 7 presents the powder pattern of the 3-1-5.4 phase. For deriving a structural model, the simulated annealing (SA) approach was used.[26] The stacking faults and low crystallinity of the sample caused the detection of false minima, leading to structural models which made no physical sense. In order to overcome that problem all local minima were extracted, resulting in a big number of possible crystal structures. Based on the similarity of the structure to the structures of the initial 3-1-8 phase and next lower hydrate phase 3-1-4.6, on the statistical distribution of the results, and on the unit cell parameters [space group $P\bar{1}$ or $P1$, a = 3.10(3) Å, b = 7.84(8) Å, c = 7.58(1) Å, α = 112.81(8)°, β = 104.3(9)°, γ = 89.9(5)°, T = 120 °C] the most probable model was chosen and presented only as an estimate of the crystal structure building motives. Unconstrained and unrestrained Rietveld refinement of that model was not possible due to the pronounced stacking faults and similar defects, which are also visually noticeable in the diffraction patterns collected at higher temperatures as presented in Figure 5.

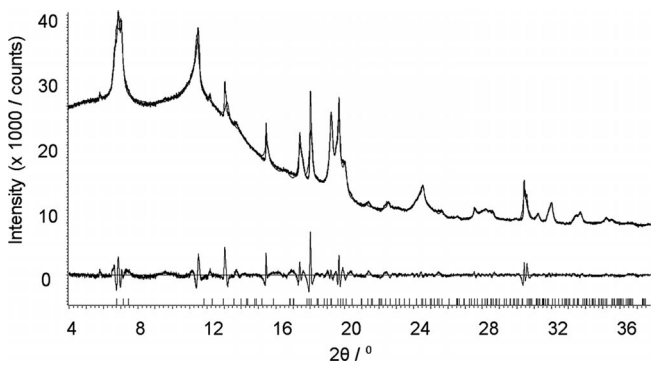

Figure 7. Pawley profile fit of the observed pattern (diamonds) of the 3-1-5.4 phase. The shape of the diffraction peaks, the background shape and misfits visible in the difference curve (*lower panel*) indicate presence of severe stacking faults and low crystallinity.

The crystal structure of the 3-1-4.6 phase was solved using SA and was subsequently refined by the Rietveld method[27] (wherein the occupancies of the atoms were constrained to the chemically obtained stoichiometry, the unconstrained refinement did not result in significantly lower figures of merit). The refinement data and the final agreement factors (R-values) are listed in Table 1, the atomic fractional coordinates and occupancy factors are given in Table 2 and the Rietveld plot is given in Figure 8. The powder pattern is characterized by strong anisotropy of width and asymmetry of the Bragg reflection. Both phenomena were satisfactory modeled by a phenomenological approach using symmetry adapted spherical harmonics. Only the peak's widths and asymmetry were treated, and no intensity correction was applied.

Table 1. Crystallographic and Rietveld refinement data for 3-1-4.6.

	3-1-4.6 phase
Molecular Formula	$3Mg(OH)_2{\cdot}MgCl_2{\cdot}4.6H_2O$
Sum formula	$Mg_4Cl_2O_{10.6}H_{14.6}$
Space Group	$P\bar{1}$ (No. 2)
Z	2
a, b, c /Å	3.158(4), 6.246(9), 7.48(1)
α, β, γ /°	95.03(4), 102.34(6), 91.86(9)
Temperature /°C	160
Density (calcd.) /g·cm^{-1}	2.116(5)
Data collection /K·min^{-1}	2
Data collection /s per frame	4
Wavelength /Å	0.826401(3)
Start and finish angle /° 2θ	5 and 30
R_{Bragg}[a)]	0.89
R_p[a)]	1.86
$R_{p'}$[a)]	15.7
R_{exp}[a)]	0.06
R_{wp}[a)]	2.48
GOF[a)]	40.3

a) R_{Bragg}, R_{wp}, R_p, R_{exp}, $R_{p'}$ and GOF are as defined in TOPAS 4.2.

Table 2. Fractional atomic coordinates and atom occupancy of the 3-1-4.6 phase.

	M WL SS[a)]	*x/a*	*y/b*	*z/c*	OCC
Mg	2 *i* 1	0.79(2)	0.402(3)	0.186(5)	1.00
O1[b)]	2 *i* 1	0.44(3)	0.59(1)	0.345(9)	1.13(4)
O2[b)]	2 *i* 1	0.87(2)	0.087(3)	0.321(5)	1.67(4)
O3[b)]	2 *i* 1	0.17(2)	0.311(9)	0.975(7)	1.38(9)

a) M: Multiplicity WL: Wyckoff Letter SS: Site Symmetry. b) The occupancies of the oxygen atoms are bigger because of the statistically distributed chlorine atoms approximately at the same positions. The scattering of the hydrogen atoms also contributes to higher electron density.

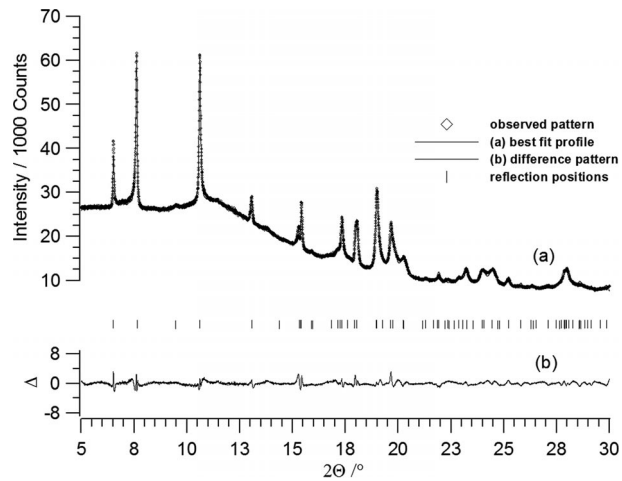

Figure 8. Scattered X-ray intensities of 3-1-4.6 phase. The observed pattern (diamonds) measured in Debye–Scherrer geometry, the best Rietveld fit profile (line) and the difference curve between the observed and the calculated profiles (below) are shown.

No attempt was made to physically model the complex peak shape suggesting severe stacking fault and other type of disorder. Further details on the crystal structure investigations may be obtained on request from the Fachinformationszentrum Karlsruhe, 76344 Eggenstein-Leopoldshafen, Germany [Fax: +49-7247-808-666;

Zeitschrift für anorganische und allgemeine Chemie ZAAC Journal of Inorganic and General Chemistry

E-mail: crysdata@fizkarlsruhe.de], on quoting the depository number CSD-426757.

Parametric Rietveld Refinement

For the parametric Rietveld refinement,[28,29] the zero error, unit cell parameters and strain contribution were refined for all patterns collectively in the temperature range from 50 to 180 °C. The background was refined for each pattern separately. The structural parameters of the published crystal structure of the 3-1-8 phase,[7] the model of the structure of the 3-1-5.4 phase and the refined structure of the 3-1-4.6 phase were kept fixed. The calculated weight percentage for each phase in the given thermal region was plotted as a function of temperature as presented in Figure 6.

Thermal Analyses

The thermal behavior of the 3-1-8 phase (8–10 mg) was studied using a TG/DTA 22 (Seiko instruments). The sample was measured in an open platinum crucible loosely covered with a platinum disk, in order to obtain the most comparable sample environment as during the X-ray data collection, wherein the sample was placed in an open capillary. The heating rate was kept to $3\ K \cdot min^{-1}$, a nitrogen flow of $300\ mL \cdot min^{-1}$. Al_2O_3 was used as reference substance for the measurements.

Acknowledgments

The authors thank the Diamond Light Source for the synchrotron beam time and the assistance of F. Adams, Dr. J. E. Parker, Dr. C. C. Tang and O. V. Magdysyuk during the measurements. D. F. thanks the Bundesministerium für Wirtschaft und Technologie (BMWi, 02E10880) for financial support.

References

[1] S. Sorel, M. Dumas, *C. R. Acad. Paris* **1976**, *65*, 102.
[2] W. Feitknecht, *Helv. Chim. Acta* **1926**, *9*, 1018.
[3] W. Feitknecht, F. Held, *Helv. Chim. Acta* **1927**, *10*, 140.
[4] W. Feitknecht, F. Held, *Helv. Chim. Acta* **1930**, *13*, 1380.
[5] W. Feitknecht, F. Held, *Helv. Chim. Acta* **1944**, *27*, 1495.
[6] C. R. Bury, E. R. H. Davies, *J. Chem. Soc. (London)* **1932**, 2008.
[7] P. M. de Wolff, L. Walter-Levy, *Acta Crystallogr.* **1953**, *6*, 40.
[8] K. Sugimoto, R. E. Dinnebier, T. Schlecht, *Acta Crystallogr., Sect. B* **2007**, *63*, 805.
[9] *Vorläufige Sicherheitsanalyse für den Standort Gorleben*, AP 9.2, Integrität geotechnischer Barrieren, GRS Braunschweig, GRS 287 and GRS 288, **2013**.
[10] W. F. Cole, T. Demediuk, *Aust. J. Chem.* **1955**, *8*, 243.
[11] S. Xia, P. Xing, S. Gao, *Thermochim. Acta* **1991**, *183*, 349.
[12] A. N. Christensen, P. Norby, J. C. Hanson, *J. Solid State Chem.* **1995**, *114*, 556.
[13] A. N. Christensen, P. Norby, J. C. Hanson, *Acta Chem. Scand.* **1995**, *49*, 331.
[14] R. E. Dinnebier, D. Freyer, S. Bette, M. Oestreich, *Inorg. Chem.* **2010**, *49*, 9770.
[15] R. E. Dinnebier, M. Oestreich, S. Bette, D. Freyer, *Z. Anorg. Allg. Chem.* **2012**, *638*, 628.
[16] R. E. Dinnebier, I. Halasz, D. Freyer, J. C. Hanson, *Z. Anorg. Allg. Chem.* **2011**, *637*, 1458.
[17] K. Sugimoto, R. E. Dinnebier, T. Schlecht, *J. Appl. Crystallogr.* **2006**, *39*, 739.
[18] T. Runčevski, C. Wu, H. Yu, B. Yang, R. E. Dinnebier, *J. Am. Ceram. Soc.,* **2013,** DOI: 10.1111/jace.12556.
[19] R. E. Dinnebier, T. Runčevski, K. Sugimoto, *Z. Anorg. Allg. Chem.* **2013**, *639*, 59.
[20] R. E. Dinnebier, M. Pannach, D. Freyer, *Z. Anorg. Allge. Chem.* **2013**, *639*, 1827.
[21] J. E. Parker, S. P. Thompson, T. M. Cobb, F. Yuan, J. Potter, A. R. Lennie, S. Alexsander, G. J. Tighe, J. A. Darr, J. C. Cockcroft, C. C. Tang, *J. Appl. Crystallogr.* **2011**, *44*, 102.
[22] S. P. Thompson, J. E. Parker, J. Potter, T. P. Hill, A. Birt, T. M. Cobb, F. Yuan, C. C. Tang, *Rev. Sci. Instrum.* **2009**, *80*, 075107.
[23] B. Hinrichsen, R. E. Dinnebier, M. Jansen, *Z. Kristallogr.* **2006**, *23*, 231.
[24] Bruker AXS, *Topas*, Version 4.2. **2007**.
[25] G. S. Pawley, *J. Appl. Crystallogr.* **1981**, *14*, 357.
[26] J. Karle, H. Hauptman, *Phys. Rev. B* **1997**, *55*, 12011.
[27] H. M. Rietveld, *J. Appl. Crystallogr.* **1969**, *2*, 65.
[28] G. W. Stinton, J. O. S. Evans, *J. Appl. Crystallogr.* **2007**, *40*, 87.
[29] A. F. Mabied, M. Muller, R. E. Dinnebier, S. Nozawa, M. Hoshino, A. Tomita, T. Sato, S. Adachi, *Acta Crystallogr., Sect. B* **2012**, *68*, 424.

Received: May 3, 2013
Published Online: October 30, 2013

